International Journal of Trend in Research and Development, Volume 2(3), ISSN: 2394-9333
www.ijtrd.com

A NOVEL METHOD FOR CAROTID ARTRY RECOGNITION USING ULTRASOUND B-MODE SCANS

[1]Swarna.G.Krishnan, [2]Mr. Senthil Kumar M.E
[1]PG scholar, [2]Assistant Professor,
M.E- Embedded system technologies,
[1,2]Sun college of Engineering and Technology,
Erachakulam, Nagercoil, Tamilnadu, India

***Abstract* - The aim of this paper is to describe a novel and completely automated technique for carotid artery (CA) recognition, far (distal) wall segmentation, and intima-media thickness (IMT) measurement, which is a strong clinical tool for risk assessment for cardiovascular diseases. The architecture of completely automated multiresolution edge snapper (CAMES) consists of the following two stages: 1) automated CA recognition based on a combination of scale-space and statistical classification in a multiresolution framework and 2) automated segmentation of lumen-intima (LI) and media-adventitia (MA) interfaces for the far (distal) wall and IMT measurement. Our database of 365 B-mode longitudinal carotid images is taken from four different institutions covering different ethnic backgrounds. The ground-truth (GT) database was the average manual segmentation from three clinical experts. The mean distance ± standard deviation of CAMES with respect to GT profiles for LI and MA interfaces were 0.081 ± 0.099 and 0.082 ± 0.197 mm, respectively. The combination of multiresolution CA recognition and far-wall segmentation led to an automated, low-complexity, real-time, and accurate technique for carotid IMT measurement. Validation on a multiethnic/multi-institutional data set demonstrated the robustness of the technique, which can constitute a clinically valid IMT measurement for assi- tance in atherosclerosis disease management.**

Keyword:Atherosclerosis; edge detection; first-order absolute moment; first-order Gaussian derivative; intima–media thickness (IMT); segmentation; ultrasound imaging.

I. INTRODUCTION

According to an old Chinese proverb, "a picture is worth a thousand words". In the modern age, this concept is still significant for computer vision and image processing, where we aim to derive better tools that give us different perspectives on the same image thus allowing us to understand not only its content, but also its meaning and significance. Image processing cannot compete with the human eye in terms of accuracy but it can perform better on observational consistency and ability to carry out detailed mathematical operations. In the course of time, image-processing research has evolved from basic low-level pixel operations to high-level analysis that now includes sophisticated techniques for image interpretation and analysis. These new techniques are being developed in order to gain a better understanding of images based on the relationships between its components, context, history, and knowledge gained from a range of sources. Digital image processing refers processing of image in digital form. Modern cameras may directly take the image in digital form but generally images are originated in optical form. They are captured by video cameras and digitized. The digitization process includes sampling and quantization. Then these images are processed by the five fundamental processes, atleast anyone of them, not necessarily all of them.

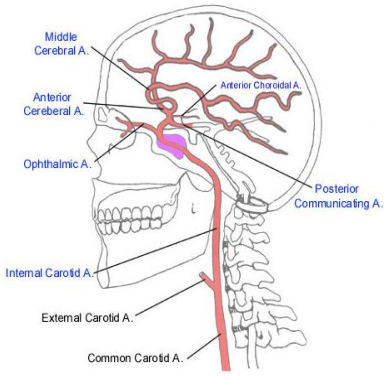

Figure.1.1. Carotid system

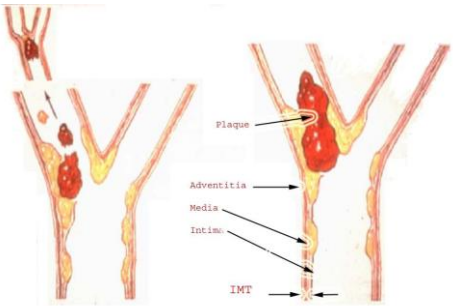

Figure.1.2. Atherosclerosis Formation

Carotid plaque is defined as a localized thickening involving the intima and media in the bulb, internal carotid, external carotid or common femoral arteries. The risk of stroke increases with the severity of carotid stenosis, and is reduced after carotid endarterectomy. The degree of internal carotid stenosis is the only well established measurement that is used to assess the risk of stroke, and it is mainly the current criterion used to decide whether carotid endarterectomy is indicated or not. It is increasingly accepted that carotid artery plaque thickness measurements, can serve as early indicators of cardiovascular disease development. In other words, it is assumed that an increased plaque thickness in the carotid artery is a predictor of future cardiovascular events like heart attack and stroke.

II. IMT MEASUREMENTS

The Intima-Media Thickness (IMT) also called Intima Medial Thickness is a measure of the thickness of

tunica intima and tunica media, the innermost layers of the wall of an artery. IMT is used to detect the presence of atherosclerotic disease in humans and, more to track the regression, arrest or progression of atherosclerosis. IMT is predictive of future cardiovascular events. The thickening of intima- media is not only due to atherosclerosis, variety of factors including local hemodynamics, shear stress, function and particle residence, time affecting the delivery and transport of potentially atherogenic particles into the arterial wall and consequent plaque formation.

The Intima–Media Thickness (IMT) of the Carotid Artery (CA) is a widely accepted and validated marker of progression of atherosclerosis and of onset of cardiovascular disorders with a predictive value for incident myocardial infarction. IMT is usually measured by using ultrasound imaging. Normally, a trained sonographer manually measures the IMT from longitudinal projections of the CA, but these manual measurement methods are time consuming, subjective, and tedious. In addition, due to the lack of standardization, the differences in the gain settings, scanner performances and the training of the clinicians all add up to cause significant variability, particularly in large and multicenter studies.

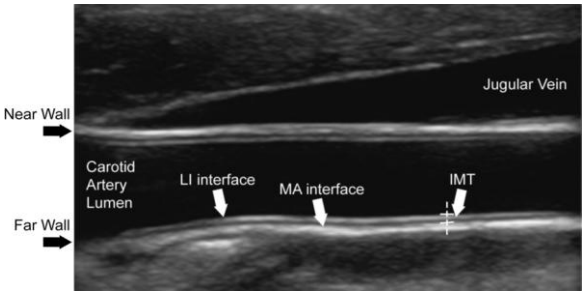

Figure 2.1. B-mode longitudinal carotid image

For the automated identification of the CA in the image frame, we need to find the edges of the AD borders using a scale–space concept in a multiresolution framework. We need fine-to-coarse downsampling followed by capturing the edges using a derivative of a Gaussian kernel with known a priori scale.

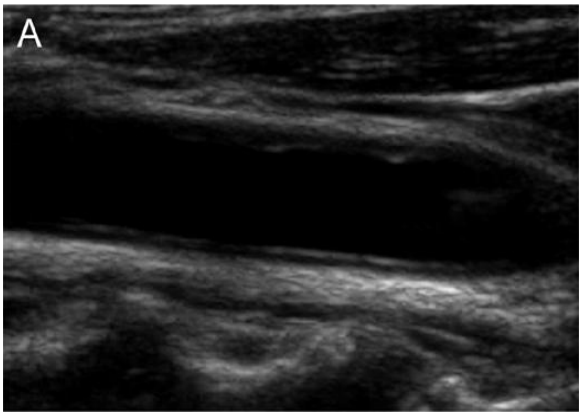

Figure 2.2. Original input image

A. Fine-to-coarse Down sampling

The image was first down sampled by a factor of 2 (the number of rows and columns of the image was halved. We implemented the down sampling method discussed by Ye et al. Adopting bucolic nterpolation that was tested on ultrasound images and showed good accuracy and a low computational cost. The interpolated value is computed by considering the 16 pixels close to the considered one. Given a point in destination image bicubic interpolation can be expressed as where is the input image and the definitions of and are and , respectively. Cubic weighting function is where function has the form.

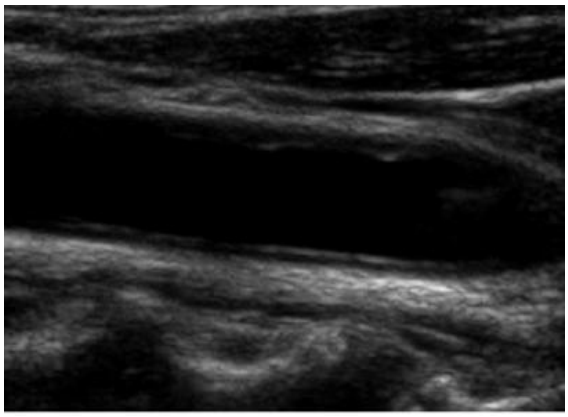

Figure 2.3. Down sampled image

Given a point (x, y) in destination image $j(x, y)$, bicubic interpolation can be expressed as

$$\mathbf{j(x,y) = \sum_{m=l}^{l+2} \sum_{n=k-1}^{k+2} I(m, n).r(m-l-dx).(dy-n+k)}$$

where $I(x, y)$ is the input image, $l=[x]$, $k=[y]$ and the definitions of dx and dy are $dx = x-l$ and $dy = y-k$

Cubic weighting r(x) is

$$\mathbf{r(x) = \frac{1}{6}[p(x+2)^3 - 4p(x+1)^3 + 6p(x)^3 - 4p(x+1)^3]}$$

where function p(x) has the form

$$p(x) = \begin{cases} x, & x > 0 \\ 0, & x \leq 0 \end{cases}$$

The multiresolution method prepares the vessel wall's edge boundary such that the vessel wall thickness tends to be equivalent to the scale of the Gaussian kernels. This infrastructure will allow scale–space-based vascular edge segmentation methods applicable to the vessel wall for edge detection, which, in turn, is necessary for locating the CA in the image frame. Note that this automated method might detect the JV border edges if they are present in the image frame. The current architecture allows a methodology to handle this challenge in case multiple edges are determined during the process of CA recognition.

B. Speckle Reduction

Noise and artifacts which can cause signal and image degradations medical image modalities.

Different image modalities exhibit distinct types of degradation. Radiographs often exhibit low contrasts while images formed with coherent energy, such as ultrasound, suffer from speckle noise. Image degradation can have a significant impact on image quality and thus affect human interpretation and the accuracy of computer-assisted methods. Poor image quality often makes feature extraction, analysis, recognition, and quantitative measurements problematic and unreliable. Therefore, image despeckling is a very important task, which motivated a considerable amount of research in medical imaging.

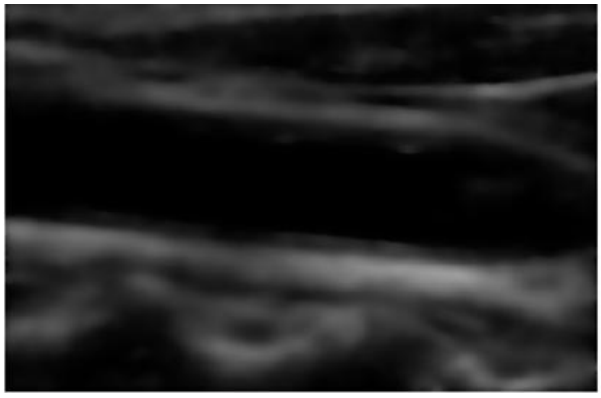

Figure 2.4. Despeckled image

Speckle noise was attenuated by using a first-order local statistics filter which gave the best performance in the specific case of carotid imaging. The despeckle filter is useful for avoiding spurious peaks during the distal (far) adventitia identification in subsequent steps. The filters utilizing first order statistics, such as the variance and the mean of the neighborhood.

C. AD_F Recognition

The despeckled image was filtered by using a first-order derivative of a gaussian kernel with scale σ and convolving with input image I(x) (where is the 2- Dvector coordinates),

$$\mathbf{F(x, \sigma) = \sigma \cdot I(x) \frac{\partial G}{\partial x} (x, \sigma)}$$

Where $\frac{\partial G}{\partial x}$ is the first- order derivative of Gaussian kernel, is the filtered image, "." denotes multiplication, and " " denotes convolution. The Gaussian kernel which had size equal to 35 * 35 pixels was defined as

$$\mathbf{G(x, \sigma) = \frac{1}{2\pi\sigma} e||x|| /2\sigma^2}$$

The scale parameter σ of the Gaussian derivative kernel was taken to be equal to 8 pixels, twice the expected dimension of the IMT value in an original fine-resolution image.

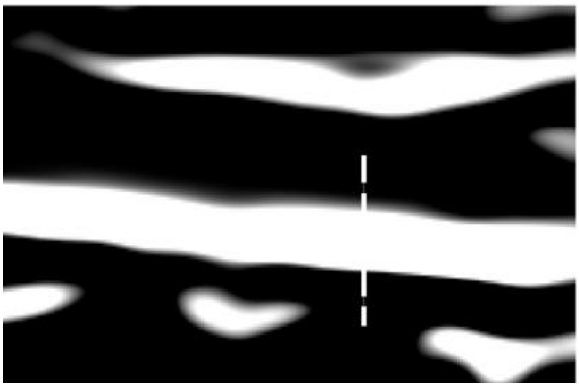

Figure 2.5. Image after convolution

Infact, an average IMT value of, e.g., 1 mm corresponds to about 12–16 pixels in the original image scale and, to 6–8 pixels in the course or down sampled image.

D. Heuristic-based automated AD_F

The proximal and distal walls are intensity maxima saturated to the value of 255. To automatically trace the profile of the distal (far) wall, we used a heuristic search applied to the intensity profile of each column. Starting from the bottom of the image (i.e., from the pixel with the higher row index, note that (0,0) is the top left-hand corner of the image), we search for the first white region where the width of the region is W_{search} pixels. The white region corresponding to the AD wall has a width of 8 pixels (equal to), which is the same size of the Gaussian kernel (as reported in the description of Step 3). A threshold value of 6-pixel width was the optimal choice for our database and ensured the correct identification of the AD in all the images. On taking the lower values, it leads to the identification of other structures that were not the far wall; such structures can be present below the carotid far wall (i.e., they are usually deeper than the artery and correspond to the neck structures around the trachea). Conversely, for higher search region pixels, we could not detect the thinner arteries in our database (i.e., the carotids having IMT lower than 05–0.6 mm, typical of healthy and young subjects). Therefore, a search region W_{search} of pixel width was the optimal choice for our database and ensured the correct identification of the AD in all the images.

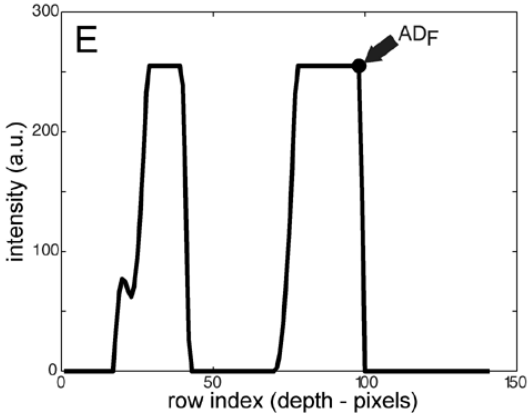

Figure.2.6 Intensity profile of the column

The deepest point of this region (i.e., the pixel with the higher row index) marked the position of the AD layer on that column. The sequence of points resulting from the heuristic search for each of the image columns constituted the overall automated AD tracing. We followed the concept of decimation of columns as adapted by Rossi *et al.* They showed that their heuristic search procedure combined with decimation ensured a faster and efficient strategy for carotid detection.

III.IMPLEMENTATION

The gray region in the 2DH represents what we consider the lumen region of the CA. Here therefore utilize the lumen region as follows. The AD points along the CA are considered one by one.

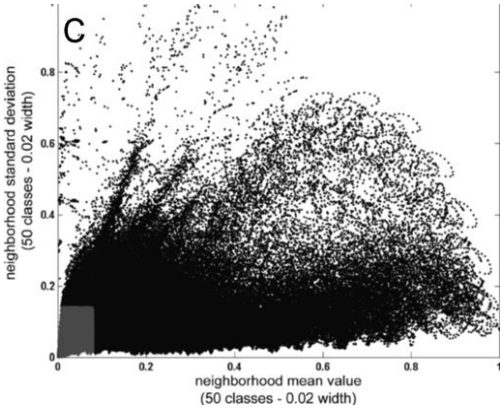

Figure 3.1. Histogram area

A. Step by Step Procedure

1) ROI estimation (ROI $_{Lumen}$) **:**We consider the sequence of the 30 pixels ROI_L above it (i.e., the 30 pixels located above the AD_F point, toward the top of the image, and, therefore, with lower row indexes).

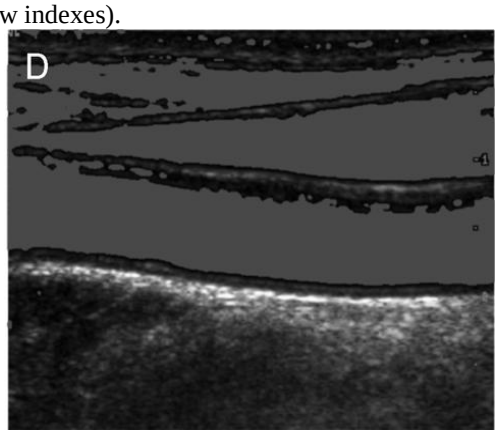

Figure 3.2. Lumen points overlaid

2) Failure of the profile point**:** We test if the ROI $_{Lumen}$ drawn around the AD_F profile points cross the lumen region and have penetrated into the lumen region by at least 15 pixels or more (let us indicate this threshold value by).

3) Tagging of profile points**:** These failed profile points must not belong to the AD_F boundary. These AD_F points that failed the lumen test are tagged as 0, whereas the rest of the points are tagged as 1. All the AD_F points that were tagged as 0 are deleted from the AD_F list.

4) The procedure is repeated for each AD_F point along the CA.

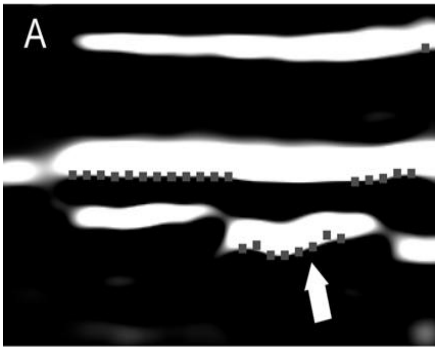

Figure 3.3 Downsampled and filtered image

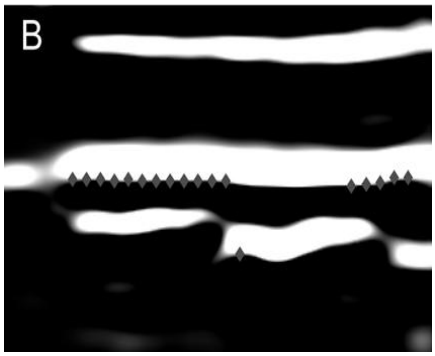

Figure 3.4 The AD points passing

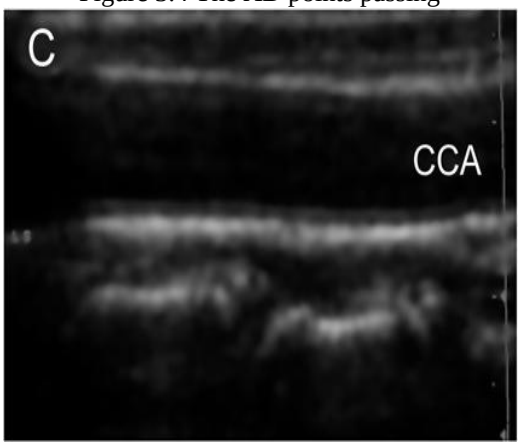

Figure 3.5 Filtered image.

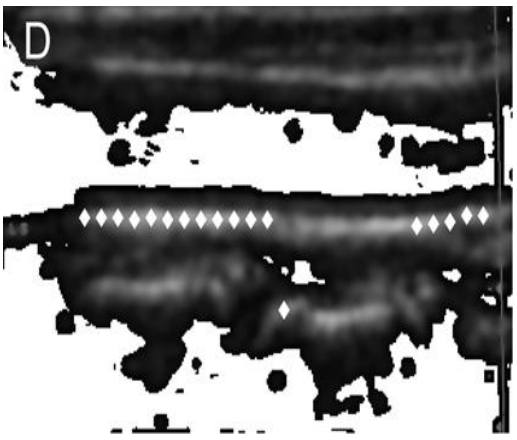

Figure 3.6 AD points (white diamonds)

The white diamonds are the AD_F points that passed the lumen test. Note that, although the lumen anatomic

information, which acts as a reference, provides a good test for catching a series of wrongly computed AD_F boundaries.

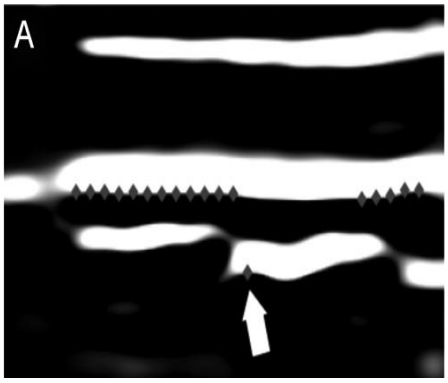

Figure 3.7 AD_F points (gray diamonds)

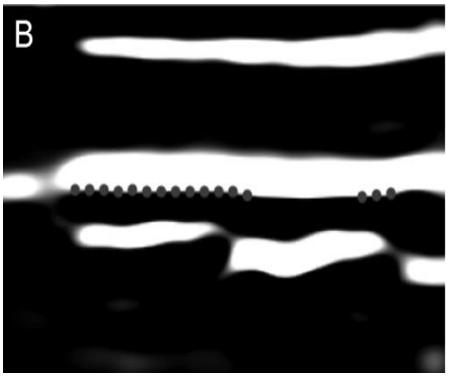

Figure 3.8. After the spike removal

B. Spike detection and removal.

Here implemented an intelligent strategy for spike detection and removal. Basically, we compute the first-order derivative of the AD_F profile and check for values higher than pixels. This value was empirically chosen by considering the image resolution. When working with images having an approximate resolution of about 0.06 mm/pixel, an IMT value of 1 mm would be about 12–16 pixels. Therefore, a jump in the AD profile on the same order of magnitude as the IMT value is clearly a spike-and-error condition. If the spike is at the very beginning of the image (first ten columns) or at the end (last ten columns), then the spiky point is simply deleted. We decided to delete spikes at the beginning or end of the image because their correction and substitution with another value would require the moving average with the neighboring points. However, spikes at the beginning or end of the image usually have too few neighboring points to perform a robust moving average. Therefore, we decided to remove them. Otherwise, all spikes are considered and either substituted by a neighborhood moving average or removed.

IV. CONCLUSION

In conclusion, CAMES, a patented class of Athero Edge(R) systems, brought automation in carotid wall segmentation and IMT measurement based on an edge-detection strategy. Among all possible techniques for automated CA location, here introduced a multiresolution approach which ensured accuracy and real-time computation. Compared with previously developed techniques multiresolution required less than 1s . Accuracy increased with respect to a previously developed automated technique (CALEX). Specifically, the IMT measurement FoM improved from 83% to about 94%. Real-time computation, robustness to noise, and complete automation make CAMES a suitable and validated clinical tool for automating and improving IMT measurement in multicenter large clinical trials.

V. FUTURE WORK

CAMES becomes very robust with respect to noise, but the LI/MA representation is less accurate. In fact, larger Gaussian kernels cause higher blurring on the LI/MA interface representation. We found that the value of 0.3 mm was suitable for all the images of the database, even if they had a different resolution. Conversely, snake performance is very dependent on the rigidity and elasticity parameters. Fine-tuning of the parameters helps in obtaining high performance but reduces applicability to diversity in the image data set due to gain settings taken by different sets of sonographers. So the future work to have an accurate representation of LI/MA by testing different filtering techniques.

REFERENCES

[1] I. M. van der Meer, M. L. Bots, A. Hofman, A. I. del Sol, D. A. Vander Kuip, and J. C. Witteman, " *Predictive value of noninvasive measures of atherosclerosis for incident myocardial infarction: The Rotterdam Study*," *Circulation*, vol. 109, no. 9, pp. 1089–1094, Mar. 9, 2004.

[2] F. Molinari, W. Liboni, P. Giustetto, S. Badalamenti, and J. S. Suri, "*Automatic Computer-based Tracings(ACT) in longitudinal 2-D ultrasound images using different scanners*," *J. Mech. Med. Biol.*, vol. 9, no.4, pp. 481–505, 2009.

[3] E. de Groot, S. I. van Leuven, R. Duivenvoorden, M. C. Meuwese, F. Akdim,M. L.Bots, and J. J. Kastelein, "*Measurement of carotid intima–media thicknessto assessprogression and regression of atherosclerosis*, " Nat. Clin. Pract. Cardiovasc. Med., vol. 5, no. 5, pp. 280–288, May 2008.

[4] F. Faita, V. Gemignani, E. Bianchini, C. Giannarelli, L. Ghiadoni, and M. Demi, "*Real-time measurement system for evaluation of the carotid intima–media thickness with a robust edge operator*," J. Ultrasound Med., vol. 27, no. 9,pp. 1353–1361, Sep. 2008.

[5] J. F. Polak, R. A. Kronmal, G. S. Tell, D. H. O'Leary, P. J. Savage, J. M. Gardin,G. H. Rutan, and N. O. Borhani, "*Compensatory increase in common carotid artery diameter. Relation to blood pressure and artery intima–media thicknessin older adults. Cardiovascular Health Study*," *Stroke*, vol. 27, no. 11, pp. 2012– 2015, Nov. 1996.

[6] J . H. Stein , C. E. Korcarz, M. E. Mays, P. S. Douglas, M. Palta, H. Zhang, T . Lecaire, D . Paine, D . Gustafson , and L . Fan, " *A semiautomated ultrasound border detection program that facilitates clinical*

measurement of ultrasound carotid intima–media thickness," J. Am. Soc. Echocardiogr., vol. 18, no. 3, pp. 244–251, Mar. 2005.

[7] D. C. Cheng, A. Schmidt-Trucksass, K. S. Cheng, and H. Burkhardt, " *Using snakes to detect the intimal and adventitial layers of the common carotid artery wall in sonographic images*," Comput. Methods Programs Biomed.,vol. 67, no. 1, pp. 27–37, Jan. 2002.

[8] S. Delsanto, F. Molinari, P. Giustetto, W. Liboni, S. Badalamenti, and J. S. Suri, *Characterization of a completely user-independent algorithm for carotid artery segmentation in 2-D ultrasound images,"* IEEE Trans. Instrum. Meas., vol. 56, no. 4, pp. 1265–1274, Aug. 2007.

[9] C. P. Loizou, C. S. Pattichis, M. Pantziaris, T. Tyllis, and A. Nicolaides , "*Snakes based segmentation of the common carotid artery intima media*," Med. Biol. Eng. Comput., vol. 45, no. 1, pp. 35–49, Jan. 2007.

[10] F. Molinari, G. Zeng, and J. S. Suri, *"An integrated approach to Compute - based automated tracing and its validation for 200 common carotid arterial wall ultrasound images: A new technique*," J. Ultrasound Med., vol.29, no. 3, pp. 399–418, Mar. 2010.